Chapter 4

Effect of Zn doping on the magneto-caloric effect and critical constants of Mott insulator MnV_2O_4

4.1 Introduction

In the previous chapter we have discussed structural, magnetic and transport properties of MnV_2O_4. In this chapter we will discuss about the Magneto caloric properties of Zn doped MnV_2O_4 and Critical behavior of MnV_2O_4 and its effect on Zn doping.

The magnetocaloric effect (MCE) has attracted much interest because of its commercial uses in magnetic refrigeration [1]. The materials showing second order magnetic transition exhibit conventional MCE and the magnetic contribution in it is of magnetic origin [2]. Moreover, the materials involving first order magnetic transition show giant MCE with significant contribution from the lattice [3]. Recently, in spinel ferromagnetic MnV_2O_4, which shows the orbital degeneracy, and the interplay of spin, orbital and lattice degrees of freedom, large magneto-caloric effect is reported around Tc (= 57 K) [4]. Other than the conventional spin-orbit coupling this interplay also arises due to the geometrical anisotropy in magnetic interaction (the so-called Kugel-Khomskii type coupling) [5]. Moreover, in these materials magnetic and structural these two phase transitions are separately observed [6–8]. This MnV_2O_4 lies in the Mott insulator regime. MnV_2O_4 exhibits a magnetic transition at T_c = 57 K (second order transition), and then a structural phase transition from a cubic to a tetragonal phase at Ts = 53 K (first order transition), with the spin structure becoming non-collinear [9]. It was also found that the structural transition could be induced by few tesla magnetic field [10, 11]. Moreover, the orbital ordering of MnV_2O_4 cannot be explained simply by anti-ferro orbital model [12]. The large magneto-caloric effect in this compound is suggested to be related to the orbital entropy change due to the change of the orbital state of V^{3+} ions with an applied field around Tc (= 57K) [4]. Furthermore, when Zn is doped on the Mn site the value of magneto-caloric effect increases and the maximum is observed at the lower transition temperature (T_S) which has been attributed to orbital ordering [13]. In this perspective the detail study of Zn doping on magneto-caloric effect of MnV_2O_4 will be interesting. Moreover, the critical behaviour, which has direct correlation with the MCE, of MnV_2O_4 might also be distinctive to provide interesting information about the magnetic spin ordering in this spinel Vanadate. Baek *et. al.* [14] have reported the critical exponents of this system. From the ac-susceptibility measurement they obtained very unusual values of

the critical constants (β = 0.36 and γ = 0.59) [14]. In a recent paper Zhang *et. al.* reported the critical constants $\beta \sim 0.349$ (close to 3D Heisenberg model) and $\gamma \sim 0.909$ (close to mean field model) [15]. Moreover, Garlea *et. al.* determined the β value from the integrated intensity I(T) fitting [16]. The I(T) can be described near the two phase transitions as $I(T) \propto (T_C,S\text{-}T)^{2\beta}$. The obtained value by them was close to 3D Heisenberg and 3D Ising models. To resolve the issue we have also studied the variation of critical constants with Zn doping using modified Arrot plots.

4.2 Experimental

The polycrystalline $Mn_{1-x}Zn_xV_2O_4$ samples were synthesized by solid state reaction technique which we have discussed in the previous chapter. The samples were characterized with X-ray powder diffraction (XRD) using Rigaku MiniFlex II DEXTOP X-ray diffractometer. The XANES measurements have been carried out at the Energy-Scanning EXAFS beamline (BL-9) in transmission mode at the INDUS-2 Synchrotron Source (2.5 GeV, 100 mA) at Raja Ramanna Centre for Advanced Technology (RRCAT), Indore, India. This beamline operates in energy range of 4 KeV to 25 KeV. The beamline optics consist of a Rh/Pt coated collimating meridional cylindrical mirror and the collimated beam reflected by the mirror is monochromatized by a Si(111) (2d = 6.2709) based double crystal monochromator. The second crystal of DCM is a sagittal cylinder used for horizontal focusing. Three ionization chambers (300 mm length each) have been used for data collection in transmission mode, one ionization chamber for measuring incident flux (I_0), second one for measuring transmitted flux (I_t) and the third ionization chamber for measuring EXAFS spectrum of a reference metal foil for energy calibration. Magnetic measurement was done using Magnetic Properties Measurement System (MPMS) SQUID (Quantum Design) magnetometer.

4.3 Results and discussion

4.3.1 Structural Analysis

4.3.1.1 X-ray diffraction

Fig. 4.1 shows the XRD patterns of $Mn_{1-x}Zn_xV_2O_4$ indicating the single phase of all the samples. We have refined the diffraction data with the Rietveld refinement program (the fitted curve has also been shown in Fig. 4.1) and the fitted parameters are shown in Table 4.1.

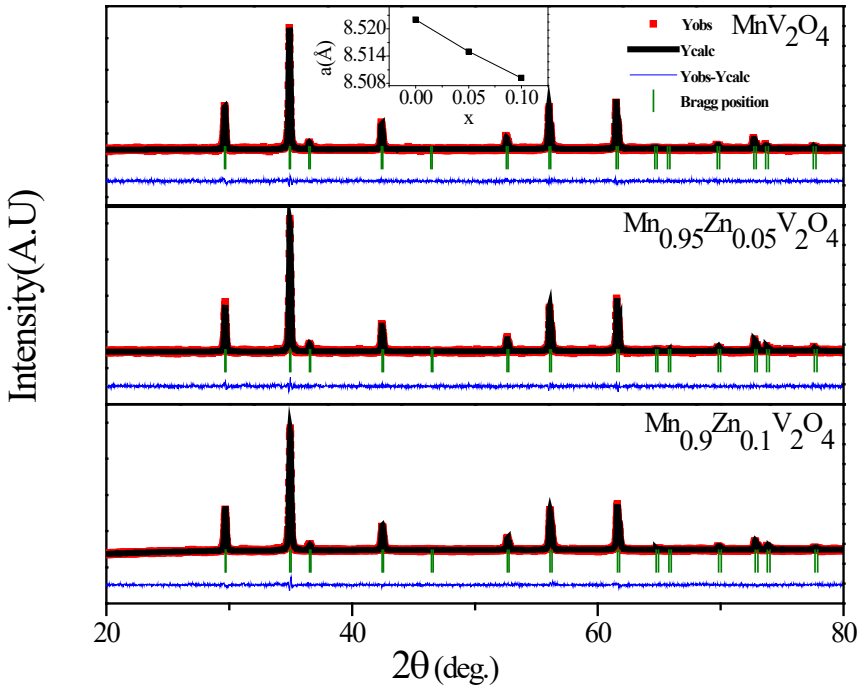

Fig. 4.1. *The X-ray diffraction pattern for the $Mn_{1-x}Zn_xV_2O_4$ (with x = 0.0, 0.05.0.1).*

The lattice parameter "a" obtained from the Rietveld refinement of the XRD data is shown as a function Zn content in the inset of Fig. 4.1. From the figure, it is clear that with increase of Zn content the lattice parameter decreases, which is due to lower ionic size of Zn^{2+} (0.74 Å) compared to Mn^{2+} (0.80 Å). The linear dependence of the lattice constant on Zn concentration indicates that there is no structural change in MnV_2O_4 with Zn doping and as a matter of fact Zn is doped into the crystal lattice following the Vegard's law [17].

Table 4.1. *Structural parameters (lattice parameters, V-V bond lengths) of $Mn_{1-x}Zn_xV_2O_4$ (with x=0, 0.05, 0.1) samples obtained X-Ray diffraction data refinement. The structural data have been refined with Space group Fd-3m at 300 K.*

	X = 0.0	X = 0.05	X = 0.1
a (Å)	8.5220(7)	8.5150(3)	8.5092(9)
V-V (Å)	3.0130 (1)	3.0105 (1)	3.0105 (1)

4.3.1.2 XANES Measurements

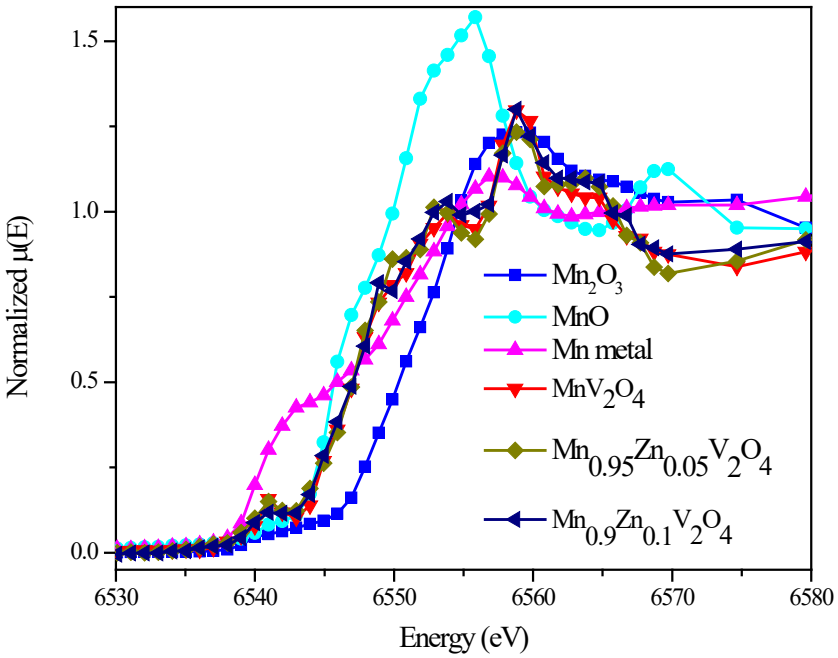

Fig. 4.2. *Normalized XANES spectra of $Mn_{1-x}Zn_xV_2O_4$ for x = 0, 0.05 & 0.1 at Mn K-edge with along with reference Mn metal, MnO and Mn_2O_3 sample.*

In order to probe the oxidation state of all the transition metals i.e. Mn, Zn and V, we have performed XANES measurements at their corresponding K edges. Fig. 4.2 shows the edge step normalized XANES spectra for Mn K-edge for the $Mn_{1-x}Zn_xV_2O_4$ (x = 0, 0.05 & 0.1) samples. The XANES spectra of all the samples are plotted with three standards Mn metal foil, MnO and Mn_2O_3 with +0, +2 and +3 oxidation state respectively. A typical K

edge XANES spectra exhibits structured pre-edge region and the dominant peak called white line peak followed by main rising edge [18]. Here, we emphasize only the main edge part of the XANES spectra for our purpose. The pre-edge features below the main edge are due to Mn 1*s* transition into unoccupied O 2*p*-Mn 3*d* (or Mn 3*d*/4*p*) hybridized states, which have *p* components projected at the Mn site as observed in many transition-metal oxides. The main edge feature at the Mn *K*-edge corresponds to the high-energy.

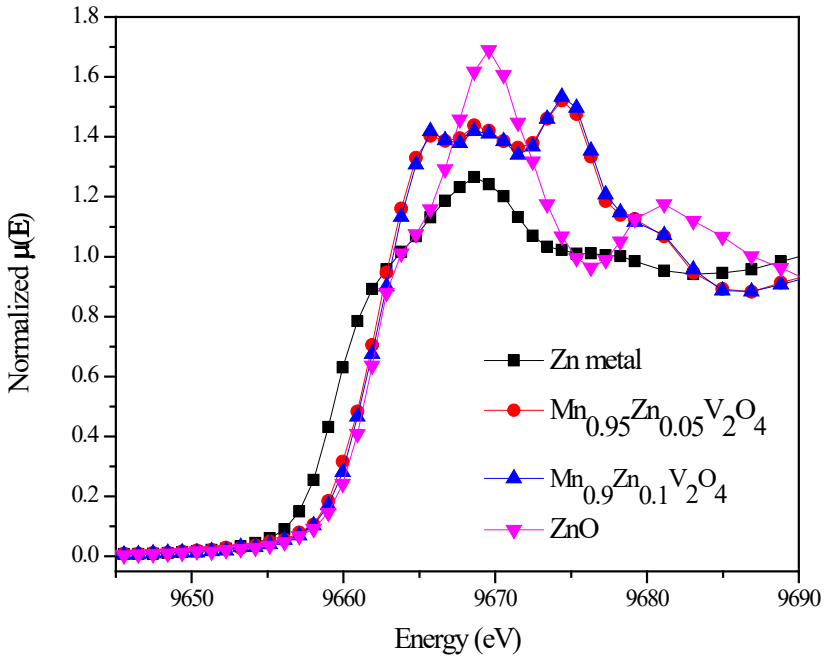

Fig. 4.3. *Normalized XANES spectra of $Mn_{1-x}Zn_xV_2O_4$ for x = 0, 0.05 & 0.1 at V K-edge with along with V metal and $VOSO_4$ standard sample.*

Fig. 4.3 shows the edge step normalized XANES spectra for Zn K-edge for the $Mn_{1-x}Zn_xV_2O_4$ for x = 0.05 and 0.1 along with two standards namely Zn metal and ZnO with +0 and +2 oxidation state respectively. This edge position in $Mn_{1-x}Zn_xV_2O_4$ for x = 0.05 & 0.1 clearly shows that Zn is present in +2 oxidation state as its edge coincide with ZnO edge.

Fig. 4.4 shows the same edge step normalized XANES spectra for V K-edge for the $Mn_{1-x}Zn_xV_2O_4$ (x = 0, 0.05 and 0.1) along with standards V metal and $VOSO_4$ with +0 and +4 oxidation state respectively. A visual inspection of Fig.4.4, the main edge energy corresponding to V K edge is close to +4 but very far from +0. Energy positions of these samples, discussed above, well matches with the earlier reports for V^{3+} [19]. A table for

their energy positions with the corresponding references is presented in Table 4.2, indicating +3 oxidation state of Vanadium in our studied samples. From the above discussion it is clear that no change in the valence states of Mn and V is occurring due to doping of Zn.

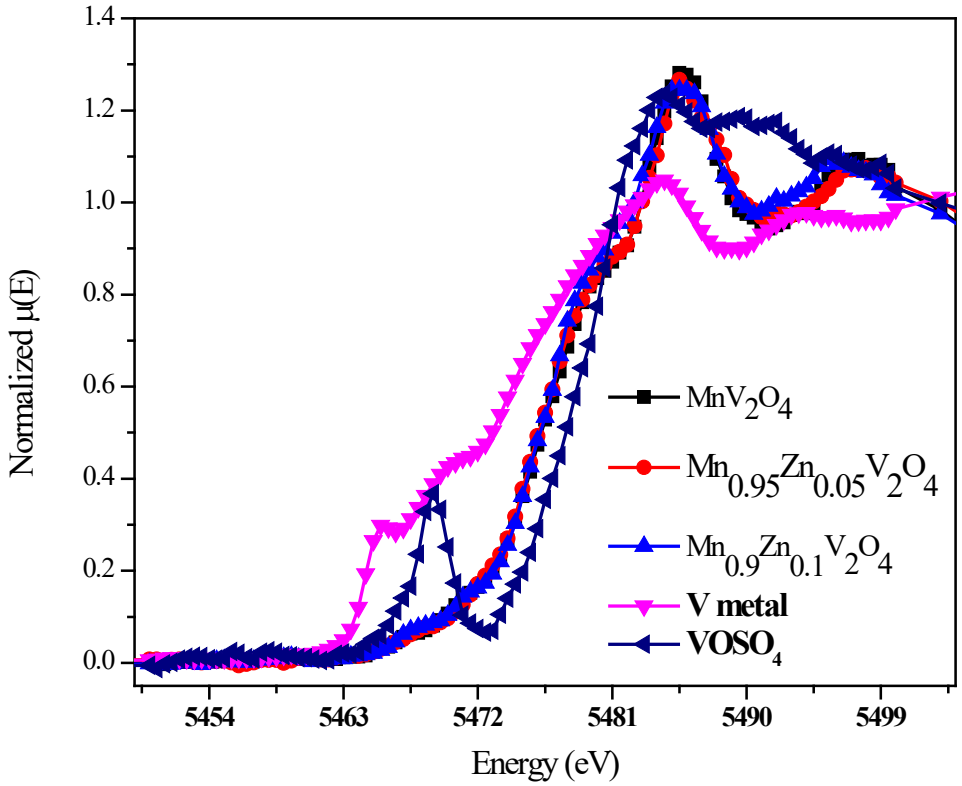

Fig. 4.4. *Normalised XANES spectra of $Mn_{1-x}Zn_xV_2O_4$ for x = 0, 0.05 & 0.1 at V K-edge with along with V metal and $VOSO_4$ standard sample.*

Table 4.2 *.Vanadium 1st derivative spectra peak energies*

V metal	V metal[3]	$V^{3+}{}_2O_3$[3]	$x = 0$	$x = 0.05$	$x = 0.10$	$V^{4+}OSO_4$
5464.60	5465	5475.7	5475.37	5475.32	5475.34	5478.13

4.3.2 Magnetic property

Fig. 4.5 shows the temperature dependence of magnetization of $Mn_{1-x}Zn_xV_2O_4$ under zero field cooled (ZFC) condition at 100 Oe. The M-T curve of MnV_2O_4 exhibits a sharp

paramagnetic ferrimagnetic (PM-FM) phase transition. It is observed that the magnetization drops sharply for all the Zn doped MnV_2O_4 samples on cooling. This is due to the spin-pairing of V-V bonds [20]. Inset of Fig. 4.5 shows the evolution of T_C with Zn content for the $Mn_{1-x}Zn_xV_2O_4$.

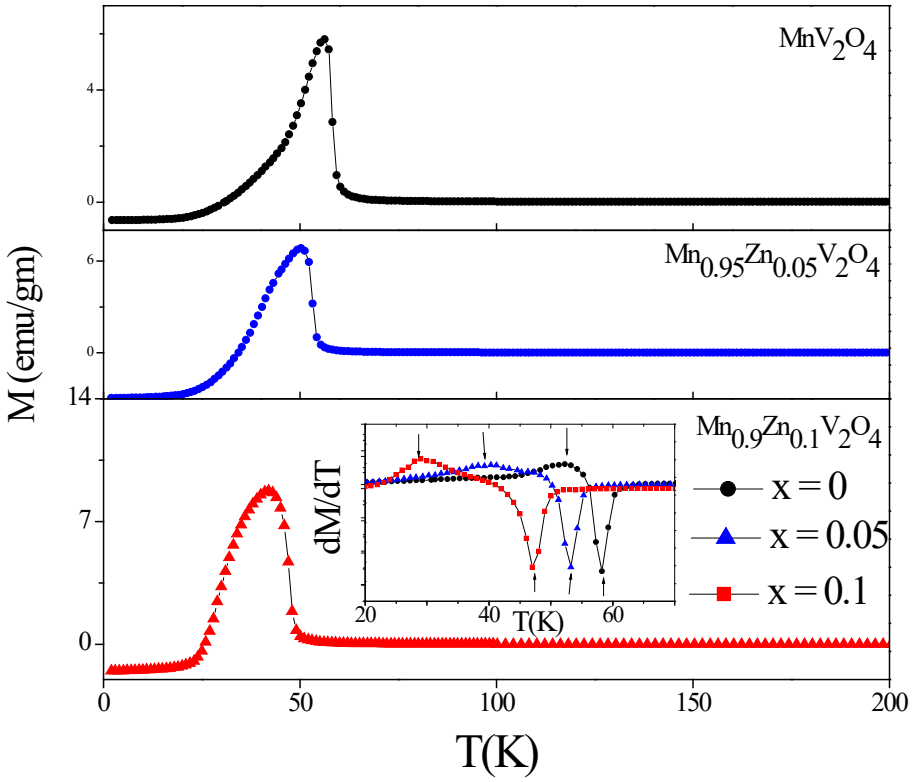

Fig. 4.5. *The temperature variation of magnetization of $Mn_{1-x}Zn_xV_2O_4$ in a 100 Oe magnetic field. Inset is showing evolution of T_c with V-V distance.*

4.3.2.1 Critical behavior

The M(H) curves at different temperatures (around the Tc) have been shown in Fig. 4.6. According to the Scaling hypothesis [21], a second order magnetic phase transition near the Curie point is characterized by a set of critical exponents of β, γ and δ and the magnetic ordering can be studied.

$$(H/M)^{1/\gamma} = C_1(T-T_c) + C_2M^{1/\beta} \qquad (4.1)$$

which combines the relations for the spontaneous magnetization below Tc

$$M\sim (T_c\text{-}T),$$

and the inverse magnetic susceptibility above Tc

$$\chi^{-1} \sim (T\text{-}T_c)$$

To find the correct values of β and γ, linear fits to the isotherms are made to get the intercepts giving M(T) and χ (T). These new values of β and γ are then used to make a new modified Arrott plot. New values of critical exponents thus obtained are re introduced in the scaling of the modified Arrott plot. The process is repeated until the iteration converges, leading to an optimum fitting value.

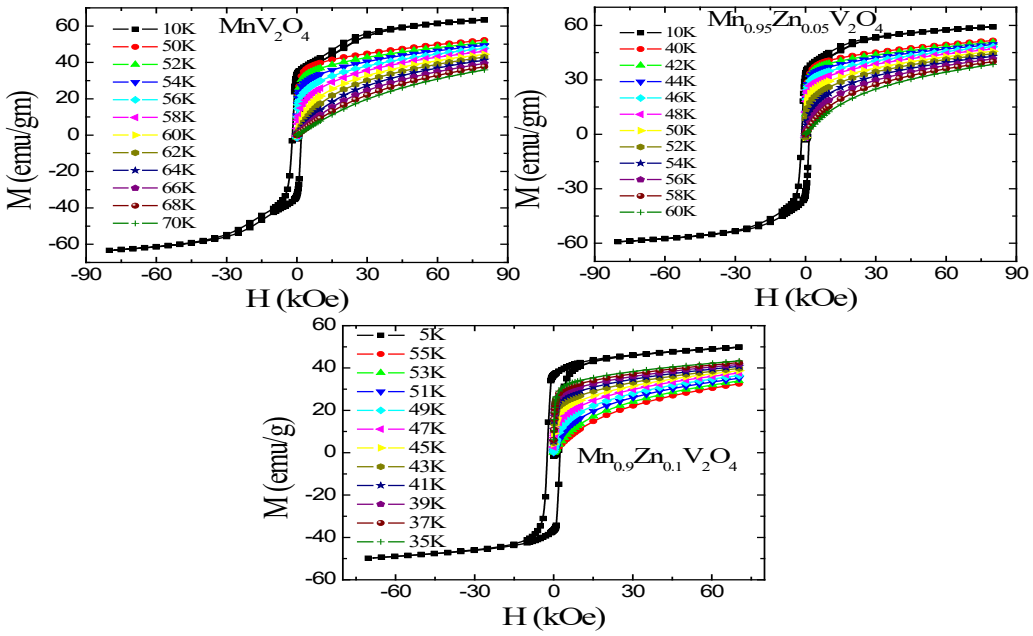

Fig. 4.6. *Magnetization as a function of applied magnetic field for the $Mn_{1-x}Zn_xV_2O_4$ (with x = 0.0, 0.05.0.1) at different temperatures (Isotherms have been measured every 2 K interval around Curie temperature)*

Fig. 4.7 shows the final result for the $Mn_{1-x}Zn_xV_2O_4$ samples. We have taken M(H) isotherms from 50 K to 70 K in every 2 K interval. The calculated values of β and γ are, respectively, 0.393 and 1.01 for x=0 sample. For x=0.05 the values are respectively, 0.40 and 1.02 whereas for x = 0.1 the values of β and γ are respectively, 0.42 and 1.07. Below 54 K it deviates from linearity due to the first order transition at ~52 K.

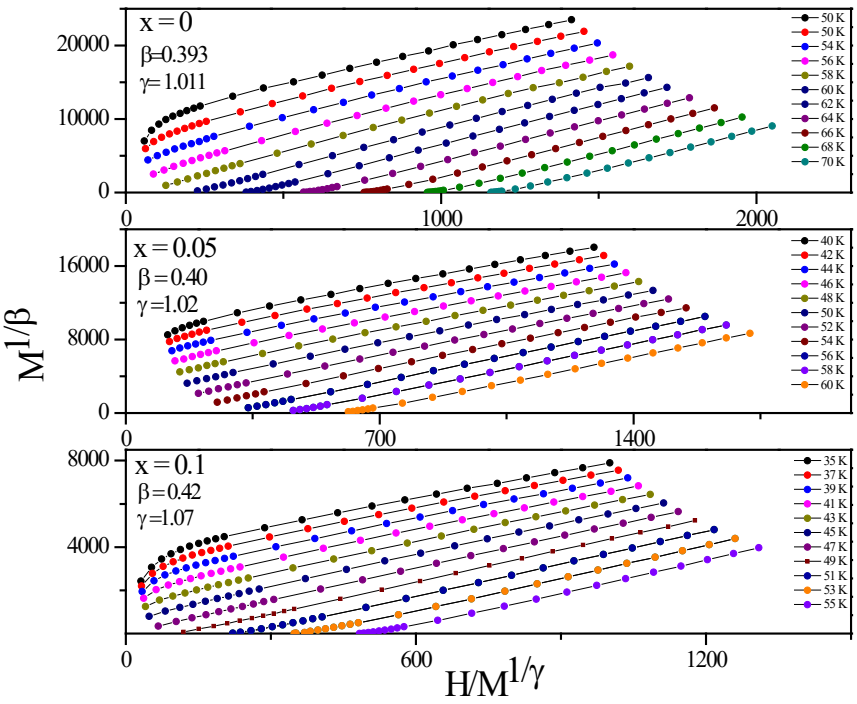

Fig. 4.7. *Final results for critical constants of $Mn_{1-x}Zn_xV_2O_4$ (with x=0, 0.05, 0.1).*

The critical values we obtained are not from the universality class. According to the scaling theory the magnetization equation can be written as $M(H,\varepsilon)\varepsilon^{-\beta} = f\pm(H/\varepsilon^{\beta+\gamma})$, where ε is the reduced temperature, f+ for T > Tc and f− for T < Tc are regular functions [22]. The equation states that the plot between $M|\varepsilon|^{-\beta}$ vs $H|\varepsilon|^{-(\beta+\gamma)}$ gives two universal curves: one for T > Tc and other for T < Tc. As shown in Fig. 4.8, the curves are divided in two parts one above Tc and one below Tc. The inset of Fig. 4.8 also shows log-log plot and this also falls into two classes one above Tc and one below Tc, in agreement with the scaling theory. Therefore the FM behaviour around Curie temperature get renormalized following the scaling equation of state indicating that the calculated critical exponents are reliable. Moreover, exponents often show various systematic trends or crossover phenomenon's one approaches Tc [23, 24]. This occurs due to the presence of various competing couplings and/or disorder. For this reason, it is useful to introduce temperature-dependent effective exponents for $\varepsilon = 0$. It can be mentioned that effective exponents are non universal properties, and they are defined as:

$$\beta^{\text{eff}}(\varepsilon) = \frac{d[\ln Ms(\varepsilon)]}{d[ln\varepsilon]} \quad . \qquad \gamma^{\text{eff}}(\varepsilon) = \frac{d[ln\chi_0^{-1}(\varepsilon)]}{d[ln\varepsilon]} \tag{4.2}$$

We have calculated the β_{eff} and γ_{eff} by using the Eq. (4.2), which do not match with universality class.

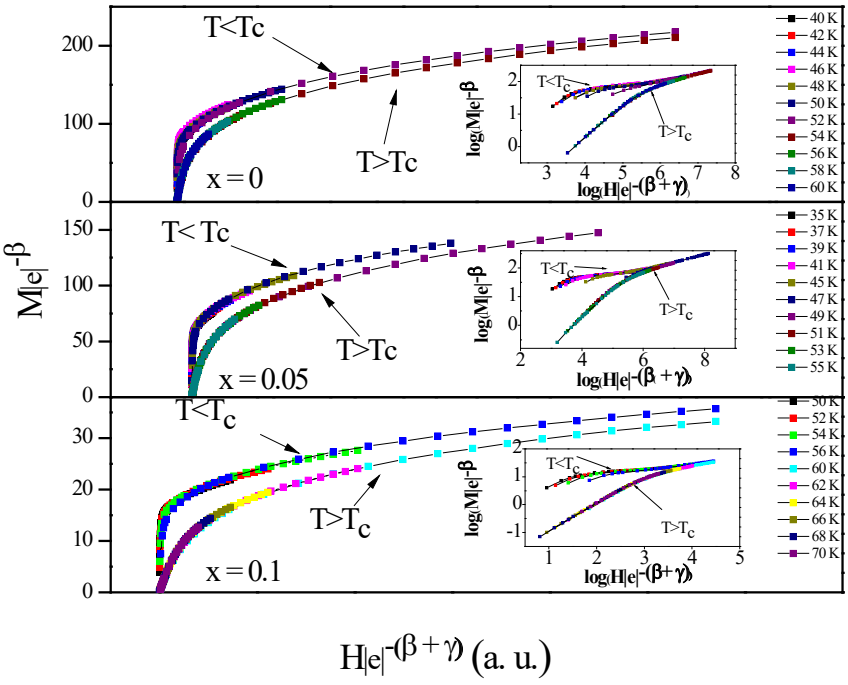

Fig. 4.8. *Universal curves and inset shows the log–log plot of universal curves of* $Mn_{1-x}Zn_xV_2O_4$ *(with x=0, 0.05, 0.1).*

It is observed from the above discussion that the critical exponents of the present investigated sample are not consistent with the universality class. The similar behavior has been observed in perovskite $Pr_{0.5}Sr_{0.5}MnO_3$ (β = 0.397and γ = 1.331) [25] and in $La_{0.7}Sr_{0.3}MnO_3$ (β = 0.45 and γ = 1.2) [26] due to phase separation. Other than perovskite, $Gd_{80}Au_{20}$ also shows unusual critical exponents (β = 0.44(2) and γ = 1.29(5)) arise due to the dilution of global spin with the substitution of non-magnetic ions [27]. In the present case very close to the second order PM-FM transition (at ~ 58 K) there exists a first order structural transition (~52 K) which is associated with the collinear to non-collinear spin transition. This may cause a large spin fluctuation which may be responsible for the unusual critical exponents between the actual material and the theoretical model.

4.3.2.2 Magneto caloric effect

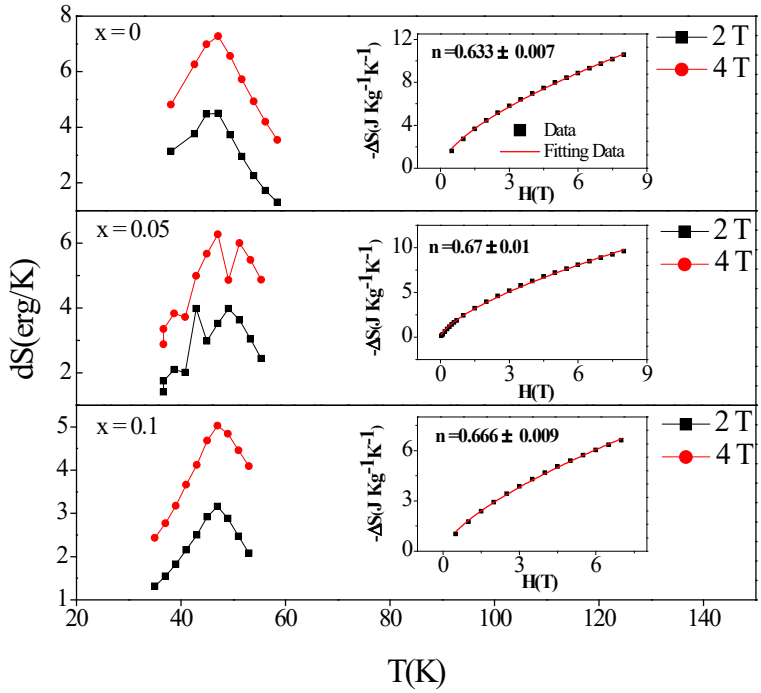

Fig. 4.9. *Magneto caloric effect of $Mn_{1-x}Zn_xV_2O_4$ at 2T and 4T magnetic fields. Inset shows the fitting of ΔS (entropy change) vs magnetic field (H) curve of $Mn_{1-x}Zn_xV_2O_4$ (with x=0, 0.05, 0.1).*

In order to further investigate we have also estimated the magneto caloric effect of all the samples. The magnetic entropy change is given by

$$|\Delta Sm| = \sum_i \frac{Mi - Mi+1}{Ti+1 - Ti} \Delta Hi \qquad (4.3)$$

Where M_i is the Magnetization at Temperature Ti [28]. The obtained |Sm| has been plotted as a function of temperature in Fig. 4.9. In the inset of Fig. 4.10 the magnetic field variation of $|S_m|$ shows the $H^{2/3}$ dependency (the value of the exponent for x = 0, 0.05 and 0.1 are respectively, 0.633, 0.67 and 0.666). This is consistent with the relation between magnetic entropy and the magnetic field near the magnetic phase transition which is given by [29]

$$|\Delta S_m| = -1.07qR(g\mu_B JH/kT_c)^{2/3} \qquad (4.4)$$

where q is the number of magnetic ions, R is the gas constant, and g is the Landau factor.

In Fig. 4.9 it is observed that as Zn content increases the magnetic entropy value decreases, which is also consistent with the Eq. (4.4). As with increase of Zn content the

magnetic Mn ions decrease. Moreover, in $Mn_{1-x}Zn_xV_2O_4$ for x = 0 and 0.1 only one peak is found and that is at Tc but for x = 0.05 two peaks are observed (one is at Tc and another is at T_{oo}). The observed behaviour for x = 0 and x = 0.05 is consistent with those reported [4,13]. It has been explained that the large magneto caloric effect in MnV_2O_4 is due to the change of the orbital state of V^{3+} ions with applied field around T_c which leads to the change in orbital entropy [4]. The observed second peak in x = 0.05 is suggested to be due to the strong coupling between orbital and spin degrees of freedom [13]. But in that case in MnV_2O_4 sample also we should get two peaks. Moreover, in the present investigation x = 0.1 sample does not show second peak. It might be the fact that in MnV_2O_4 the two transitions are very close to each other and because of that two peaks overlap into a single peak. Moreover for 10% Zn doping the chemical pressure increases which reduces the residual spins on the V-V pairs which leads to the decrease of long range magnetic ordering. As a matter of fact the coupling between orbital and spin degrees of freedom decreases. This might be the reason of diminishing the peak at low temperature when 10% Zn is doped.

4.4. Conclusion

The XANES study indicates that no change in the valence states of Mn and V is occurring due to doping of Zn and V remains in 3+ state. The giant magneto-caloric effect value is observed in these spinel vanadates and the entropy change (MCE value) decreases with increase of Zn content. It has been shown that the obtained values of the critical exponents β, γ and δ do not belong to universal class and the values are in between the 3D Heisenberg model and mean field interaction model. The magnetization data follow the scaling equation and collapse into two branches indicating that the calculated critical exponents and critical temperatures are unambiguous and intrinsic to the system. The observed double peaks in MCE of $Mn_{0.95}Zn_{0.05}V_2O_4$ are due to the strong coupling between orbital and spin degrees of freedom. In this composition (x = 0.05) the orbital ordering becomes maximum which in effect increase the coupling between orbital and spin degrees of freedom at T_{oo} leading the second peak in magneto-caloric behavior in x = 0.05 sample. When Zn content increases (*viz.* x = 0.1) the chemical pressure increases which reduces the

residual spins on the V-V pairs which leads to the decrease of long range magnetic ordering. As a consequence coupling between orbital and spin degrees of freedom decreases.

References

[1]. Tishin, A. M. and Spichkin, I., The Magnetocaloric Effect and Its Applications, Institute of Physics Publishing, Bristol, 2003.

[2]. Pecharsky, V. K., Gschneidner K. A., Pecharsky, A. O. and Tishin, A. M., Thermodynamics of the magnetocaloric effect, Phys. Rev. B, 64, 144406/1-144406/13, 2001.

[3]. Campos, A. D., Rocco, D. L, Carvalho Alexandre, M. G., Caron, L., Coelho A. A., Gama S., Silva, L. M. d., Gandra, F. C. G., Santos, A. O. d., Cardoso, L. P., Ranke, P. J. v. and Oliveira, N. A. d., Ambient pressure colossal magnetocaloric effect tuned by composition in $Mn_{1-x}Fe_xAs$, Nat. Mater., 5, 802-804, 2006.

[4]. Luo, X. , Sun, Y. P., Hu, L., Wang, B. S., Lu, W. J., Zhu, X. B.,Yang, Z. R and Song, W. H., Observation of the large magnetocaloric effect in an orbital–spin-coupled system MnV_2O_4 , J. Phys. Condens. Matter, 21, 436010/1-436010/5, 2009.

[5]. Kugel, K. I. and Khomskii, D. I., Crystal structure and magnetic properties of substances with orbital degeneracy, J. Exp. Theo. Phys. 37, 725-730, 1973.

[6]. Mamiya, H., Onoda, M., Furubayashi, T., Tang, J. and Nakatani, I., Structural and magnetic studies on vanadium spinel MgV_2O_4, J. Appl. Phys., 81, 5289-5291, 1997.

[7]. Ueda, Y. and Fujiwara, N., Magnetic and Structural Transitions in $(Li_xZn_{1-x})V_2O_4$ with the Spinel Structure. J. Phy. Soc. Jpn., 66, 778-783, 1997.

[8]. Nishiguchi, N. and Onoda, M., A pseudotetramer in the geometrically frustrated spinel system CdV_2O_4 . J. Phys. Condens. Matter, 14, L551-L557, 2002.

[9]. Plumier, R. and Sougi, M., Observation of a first order transition in the ferrimagnetic spinel MnV_2O_4, Solid State Commun., 64, 53-55, 1987.

[10]. Adachi, K., Suzuki, T., Kato, K., Osaka, V., Takata, M. and Katsufuji, T., Magnetic-Field Switching of Crystal Structure in an Orbital-Spin-Coupled System:MnV_2O_4, Phys. Rev. Lett., 95, 197202/1-197202/4, 2005.

[11]. Suzuki, T., Katsumura, M., Taniguchi, K., Arima, T. and Katsufuji, T., Orbital Ordering and Magnetic Field Effect in MnV_2O_4, Phys. Rev. Lett., 98, 127203/1-127203/4, 2007.

[12]. Chung, J. H., Kim, J. H., Lee, S. H., Sato, T. J., Suzuki, T., Katsumura, M. and Katsufuji, T., Magnetic excitations and orbital physics in the ferrimagnetic spinels MnB_2O_4 (B=Mn,V), Phys. Rev. B, 77, 054412/1-054412/5, 2008.

[13]. Luo, X. , Sun, Y. P., Lu, W. J., Zhu, X. B., Yang, Z. R. and Song, W. H., Observation of the large orbital entropy in Zn-doped orbital-spin-coupled system MnV_2O_4, Appl. Phys. Lett., 96, 062506/1-062506/3, 2010.

[14]. Baek, S. H., Choi, K. Y., Reyes, A. P., Kuhns, P. L., Curro, N. J., Ramanchandran, V., Dalal, N. S., Zhou, H. D. and Wiebe, C. R., Ac susceptibility and ^{51}V NMR study of MnV_2O_4, J. Phys. Condens. Matter, 20, 135218/1-135218/6, 2008.

[15]. Zhang, L., Han, H., Qu, Z., Fan, J., Ling, L., Zhang, C., Pi, L. and Zhang, Y., Critical behavior of spinel MnV_2O_4 investigated by dc-magnetization, J. Appl. Phys., 115,233910/1-233910/5, 2014.

[16]. Garlea, V. O., Jin, R., Mandrus, D., Roessli, B., Huang, Q., Miller, M., Schultz, A. J. and Nagler, S. E., Magnetic and Orbital Ordering in the Spinel MnV_2O_4, Phys. Rev. Lett., 100, 066404/1-066404/4, 2008.

[17]. Luo, J., Liang, J. K., Liu, Q. L., Liu, F. S., Zhang, Y., Sun, B. J. and Rao, G. H., Structure and magnetic properties of Mn-doped ZnO nanoparticles, J. Appl. Phys. 97, 086106/1-086106/3, 2005.

[18]. Singh, H., Ghosh, H., Rao, T. V. C. and Sinha, A. K., Coexistence of Co3+ and Co2+ in ceramic Co_3TeO_6; XANES, Magnetization and first principle study, arXiv:1404.1658 [cond-mat.mtrl-sci], 2014.

[19]. Wong, J. , Lytle, F. W., Messmer, R. P. and Maylotte, D. M., X-edge absorption spectra of selected vanadium compounds, Phys. Rev. B, 30, 5596-5610, 1984.

[20]. Blanco-Canosa, S., Rivadulla, F., Pardo, V., Baldomir, D., Zhou, J. S., García-Hernández, M., López-Quintela, M. A., Rivas, J. and Goodenough, J. B., Enhanced Pressure Dependence of Magnetic Exchange in AV_2O_4 Spinels Approaching the Itinerant Electron Limit, Phys. Rev. Lett., 99,187201, 2007.

[21]. H. E. Stanley, Introduction to phase transitions and critical phenomenon, Oxford University press, New York, 1971.

[22]. Kaul, S. N., Static critical phenomena in ferromagnets with quenched disorder, J. Magn. Magn. Mater., 53, 5-53, 1985.

[23]. Perumal, A. , Srinivas, V., Rao, V. V. and Dunlap, R. A., Quenched Disorder and the Critical Behavior of a Partially Frustrated System, Phys. Rev. Lett., 91, 137202/1-137202/4, 2003.

[24]. Srinath, S., Kaul, S. N. and Sostarich, M.-K., Isotropic-Heisenberg to isotropic-dipolar crossover in amorphous ferromagnets with composition near the percolation threshold, Phys. Rev. B, 62, 11649-11660, 2000 and references therein.

[25]. Pramanik, A. K. and Banerjee, A., Critical behavior at paramagnetic to ferromagnetic phase transition in Pr0.5Sr0.5MnO3:A bulk magnetization study, Phys. Rev. B, 79, 214426/1-214426/7, 2009.

[26]. Taran, S. Chaudhuri, B. K., Yang, H. D., Neeleshwar, S., Chen, Y. Y. and Chatterjee, S., Critical exponents of the $La_{0.7}Sr_{0.3}MnO_3$, $La_{0.7}Ca_{0.3}MnO_3$, and $Pr_{0.7}Ca_{0.3}MnO_3$ systems showing correlation between transport and magnetic properties, J. Appl. Phys., 98, 103903/1-103903/6, 2005.

[27]. Poon, S. J., and Durand, J., Critical phenomena and magnetic properties of an amorphous ferromagnet: Gadolinium-gold, Phys. Rev. B, 16, 316-330, 1977.

[28]. Fan, J. , Ling, L., Hong, B., Pi, L. and Zhang, Y., Magnetocaloric effect in perovskite manganite, J. Magn. Magn. Mater., 321, 2838-2841, 2009.

[29]. Oesterreicher, H. and Parker, F. T., Magnetic cooling near Curie temperatures above 300 K, J. Appl. Phys., 55, 4334-4338, 1984.